JOURNAL OF GUIDANCE, CONTROL, AND DYNAMICS
Vol. 23, No. 1, January–February 2000

Space-Based Visible Space Surveillance Performance

Jayant Sharma*
Lincoln Laboratory, Massachusetts Institute of Technology, Lexington, Massachusetts 02420

The Space-Based Visible sensor package on the Midcourse Space Experiment satellite has been used to conduct space surveillance experiments for nearly one and a half years. The long-term detection sensitivity and metric performance of Space-Based Visible using onboard signal processed data are described. These data are also used to illustrate unique capabilities of the Space-Based Visible sensor. Space-Based Visible has access to the entire geosynchronous belt, and its wide field of view allows data to be collected on multiple resident space objects simultaneously. The large field of view also allows data to be collected on uncorrelated targets. Use of Space-Based Visible observations to detect and identify uncorrelated targets is also presented.

Introduction

THE goal of Space-Based Visible (SBV) is to demonstrate the ability to make observations of resident space objects (RSOs) from a space-based platform. The description of the data processing is provided in a previous paper.[1] Sensor characteristics relevant to routine space surveillance are summarized in Table 1. This paper describes how the unique properties of the SBV sensor can be exploited for space surveillance. First, the SBV sensor is on an orbiting platform and has access to the entire geosynchronous belt. Second, the wide field of view of the sensor allows multiple RSOs to be detected simultaneously.

Surveillance Data Summary

This section describes the quality of SBV surveillance data. SBV has been observing RSOs since its launch in April 1996, and these data are used to describe the quality of the space surveillance observations. Unless noted otherwise, all of the SBV data used in this study are routine space surveillance experiment data. These data are collected in a sidereal track mode, where the stars appear as point sources and the RSOs appear as streaks. Routine surveillance experiment data are then processed through the onboard signal processor to extract the star and streak information as shown in Fig. 1.

The ability of SBV to detect a large range of objects, and the metric accuracy of those observations, will be illustrated. Over 10,000 observations of RSOs have been collected, and the histogram of the observed SBV magnitude of these detections is shown in Fig. 2b. Because the primary focus of SBV is deep space surveillance, over 95% of these observations are on deep space objects. SBV magnitude closely approximates the visual magnitude scale, but is a function of the sensitivity of the SBV charged-coupled device (CCD) over its spectral range. Figure 2b clearly demonstrates a detection sensitivity down to 15th SBV magnitude for the sidereal mode of data collection. Figure 2a indicates the predicted detection sensitivity of SBV for deep space RSOs and a signal-to-noise ratio of six for various background levels (T. P. Opar, Lincoln Laboratory, Massachusetts Institute of Technology, Lexington, Massachusetts, June 1999). The SBV sensor is performing slightly above the predicted sensitivity. Figures 3 and 4 illustrate the histogram of observed magnitudes for selected RSOs. These two nonstabilized geosynchronous satellites illustrate the range of detections due to different viewing angles of a large and small RSOs.

The goal of the SBV sensor is to produce metric observations that have a 4-arc-s metric accuracy. This is accomplished in three primary steps. First, the pointing of the sensor is accurately estimated. This is done by centroiding the detected star location and matching them with stars from a catalog. The second step involves precisely determining the location of streak endpoints on the focal plane and mapping them back into right ascension and declination.[1] Finally, the position of the SBV platform must be accurately determined. This is accomplished by performing precise orbit determination of MSX.[2] Figure 5 shows the quality of the SBV pointing and the MSX orbit for the first 500 days of SBV operations. Figure 5a shows a histogram of the rms star fit residuals per frameset and indicates that the average star match with a catalog star is performed with a precision of 0.8 arc-s. Because the pointing is determined by a least-squares estimation process, the pointing accuracy can be approximated by dividing the star match quality by the square root of the number of stars matched. With an average of 12 stars being matched per frameset, the resulting pointing accuracy is approximately 0.2 arc-s. Figure 5b is a histogram of the Millstone radar rms range residuals and illustrates that the orbits are known to better than 10 m. The radar data are not used to estimate the orbit and serve as an independent assessment of the orbit quality.[3]

The updated SBV pointing is used to map streak endpoints from focal plane coordinates to right ascension and declination coordinates, which are then combined with the MSX location to create space-based observations. The accuracy of these observations is assessed by calculating the difference between the observed location and an accurate predicted location. The predicted location is based on an orbit using the ground based Space Surveillance Network (SSN) observations.[3] This assessment relies on an accurate orbit using SSN data, which is not always available due to the quality and/or quantity of tracking data. For this analysis, SBV observations of Russian navigation satellites (GLONASS) were used for the accuracy assessment. These are noncalibration satellites that are routinely tracked by both optical and radar sensors. A histogram of the SBV rms observation residuals for GLONASS satellites is shown in Fig. 6, and indicates that the accuracy of the observations is approximately 4 arc-s. Table 2 summarizes the postflight predicted metric accuracy and indicates that the metric accuracy achieved is slightly lower than that predicted. The temporal behavior of orbit and observation quality is shown in Fig. 7 and shows no degradation over the time period indicated.

Geosynchronous Belt Surveillance

The quality and sensitivity of the SBV data have been discussed in the preceding section. This section will look at some of the capabilities of SBV in performing space surveillance. In particular, this section will look at exploiting the wide field of view (1.4 × 1.4 deg) and the ability of the SBV to view the entire geosynchronous belt. Access to the entire geosynchronous belt is shown in Fig. 8, which shows a plot of all station-kept geosynchronous satellites observed by SBV through November 1997. The tick marks indicate location as a function of east longitude on the geosynchronous belt.

Figure 8 shows that SBV has access to the entire geosynchronous belt. The wide field of view allows multiple objects to be detected. This is particularly advantageous for surveillance of the geosynchronous belt, where satellites are stationed close together. The wide field of view also allows for the detection of nonstation-kept RSOs

Received 16 November 1998; revision received 12 July 1999; accepted for publication 3 August 1999.

*Technical Staff Member, Surveillance Techniques Group.

Table 1 SBV sensor characteristics

Property	Value
Spectral range	0.3–0.9 μm
Spatial resolution	12.1 arc-s/pixel
Field of view per CCD	1.4 × 1.4 deg
Aperture, f-number	15 cm, f/3
Number of frames per frameset	4–16
Frame integration times	0.4, 0.625, 1, 1.6 s
Frame sizes	420 × 420, 357 × 420 pixels

in the geosynchronous belt. This capability is shown in Fig. 9a, which shows a cluster of five commercial communication satellites located at 259°E longitude as well as a drifting RSO. Figure 9b shows an histogram of the observed location of the satellites in this cluster over several hundred days and clearly shows the small station-keeping bounds used by these satellites. The location on the geosynchronous belt is calculated by converting the observations directly to longitude. The position vector of the RSO relative to SBV is calculated by multiplying the unit vector of the observed direction by the range to the RSO, as determined from the correlated element set. The inertial position vector of the RSO relative to the center of the Earth is determined by adding the precise position of SBV to

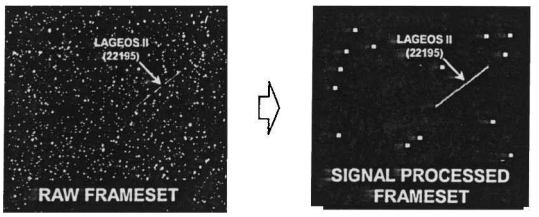

Fig. 1 Routine surveillance data.

Table 2 Postflight predicted metric accuracy

Error sources	Nominal value, arc-s
Ephemeris, 15 m	1.0
Timing, 1 ms	0.6
Boresight pointing	0.2
SEP determination	1.2
Total RSS error	1.7

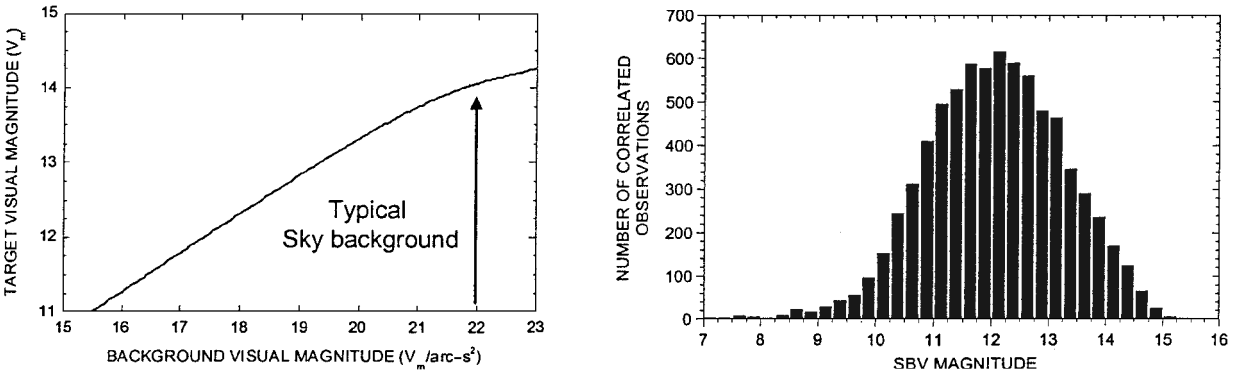

Fig. 2 Predicted and observed SBV magnitude of correlated RSOs.

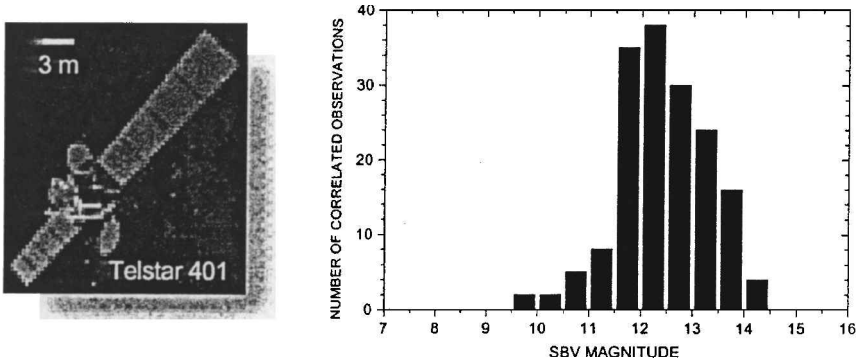

Fig. 3 Observed magnitude of 22927 (Telstar 401).

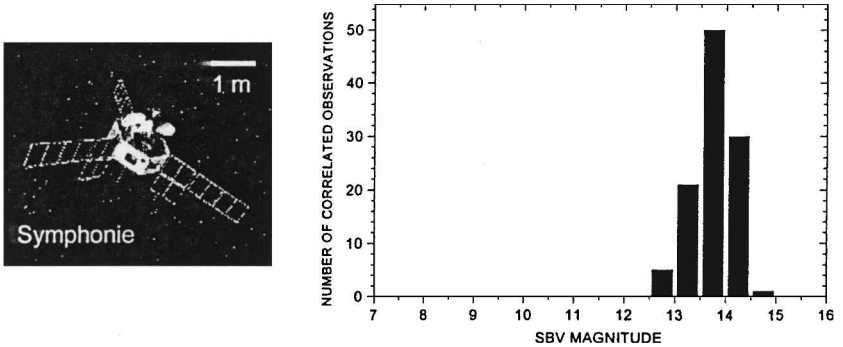

Fig. 4 Observed magnitude of 7578 and 8132 (Symphonie A and B).

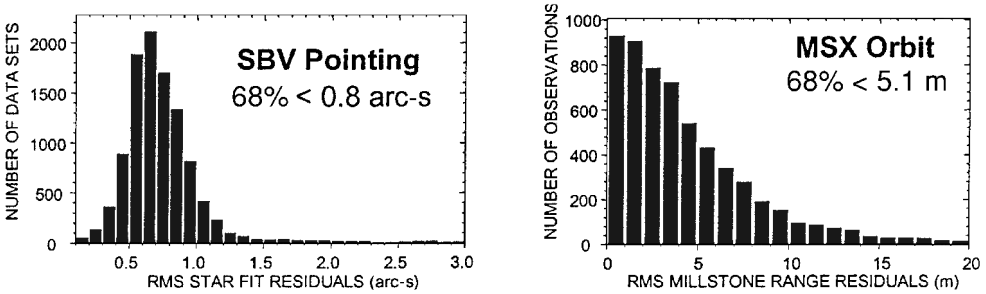

Fig. 5 SBV pointing and MSX orbit quality.

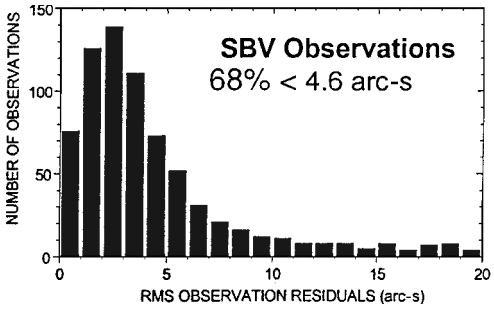

Fig. 6 SBV observation residuals.

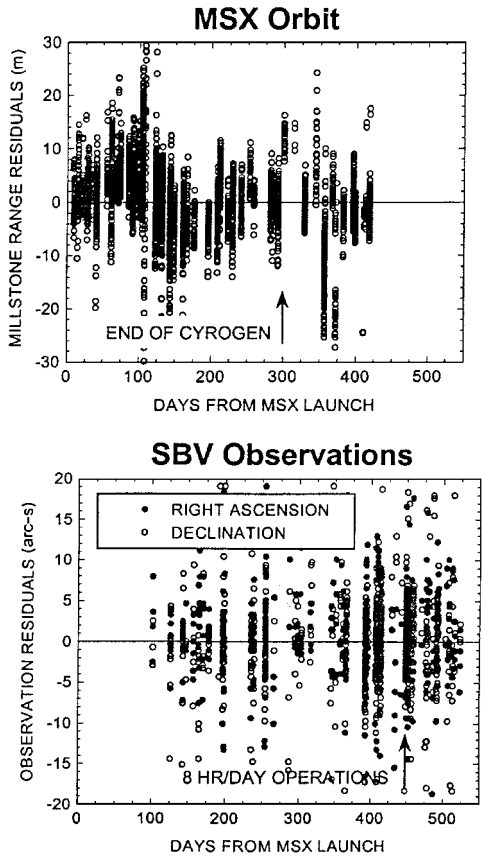

Fig. 7 Temporal variation of orbit and observation quality.

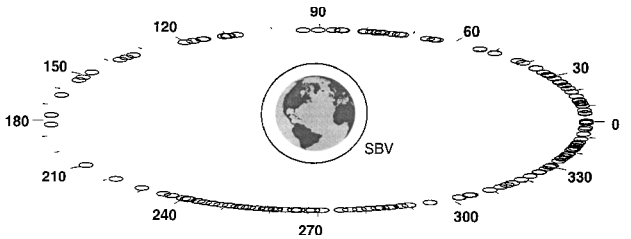

Fig. 8 All station-kept geosynchronous satellites observed by SBV (as of November 1997).

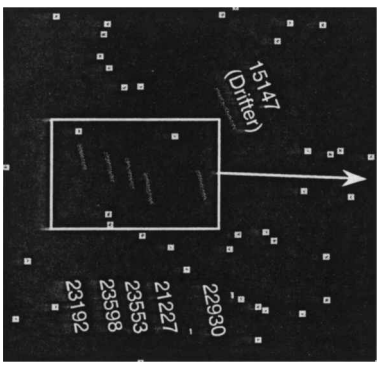

a)

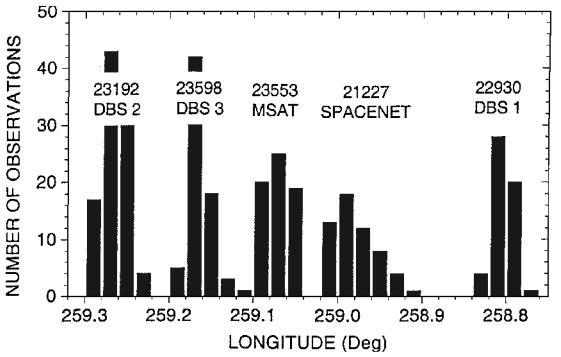

b)

Fig. 9 SBV observations of a geosynchronous cluster.

the SBV–RSO position vector. This geocentric vector is then rotated into an Earth-fixed frame and converted to longitude and latitude. By relying on the element set for only the range value, additional position errors in the element set are not mapped into longitude or latitude.

The observed location of geosynchronous satellites is also useful in detecting station-keeping maneuvers of the satellite. If the satellite is observed frequently, then a maneuver can be detected by looking at the change in longitude. Figure 10a shows a cluster of two Russian geosynchronous RSOs located at 12°E longitude, with two additional drifters in the field of view. Figure 10b shows a plot of the observed longitude as a function of time, and longitudinal station-keeping maneuvers are visible. Two maneuvers for object 22269 are evident at an interval of approximately 50 days. Similarly, two maneuvers are visible for object 22557 but are separated by 80 days. Knowledge of the maneuvers can be utilized to restart the orbit determination process and thus improve the orbit accuracy or can be used to estimate the size of the maneuver if precise orbit determination procedures are used.

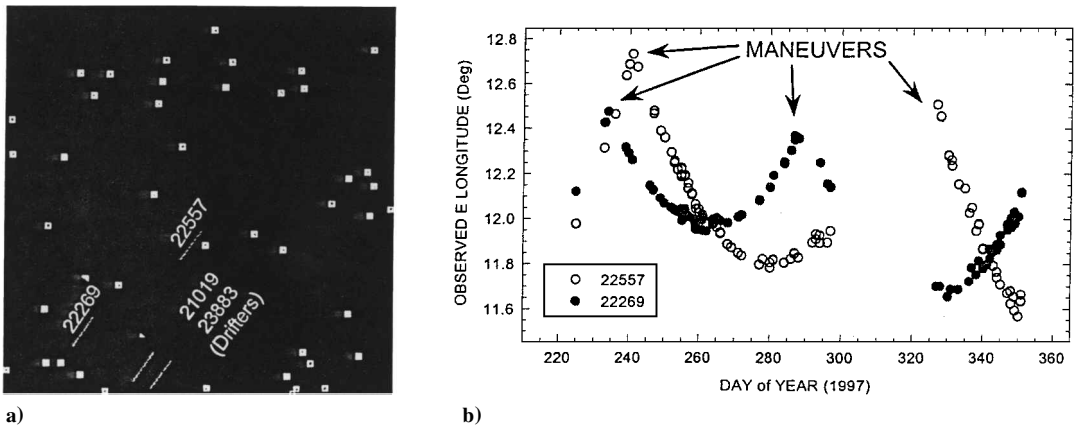

Fig. 10 SBV observations of maneuvering geosynchronous satellites.

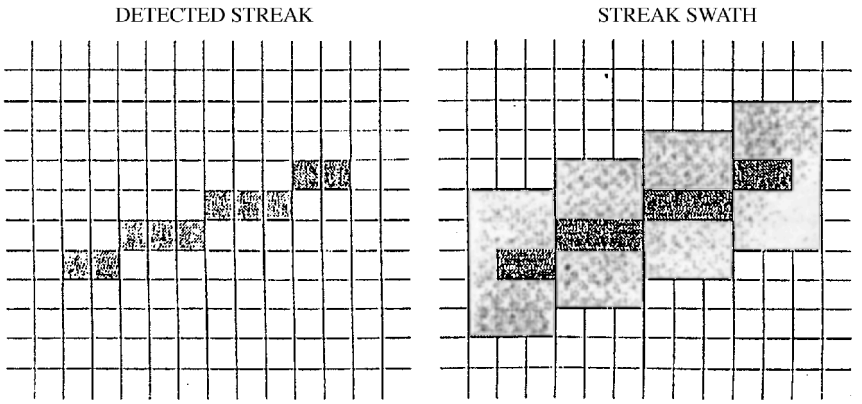

Fig. 11 Streak swath.

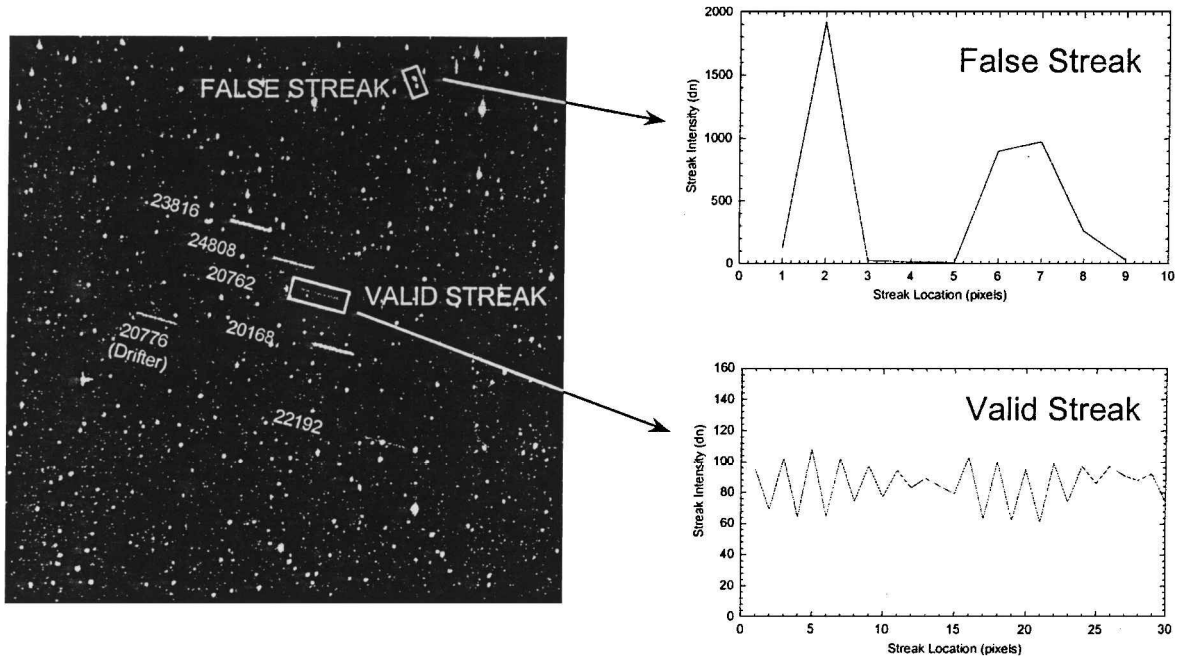

Fig. 12 Determination of valid streaks.

Uncorrelated Target Analysis

This section looks at another benefit of a wide field of view sensor: its ability to collect data on lost objects and objects whose element sets are not well known. In addition to collecting data on known objects, a wide field of view also facilitates the detection of uncorrelated targets (UCTs). Before the SBV UCT data can be utilized, it is necessary to first determine if the detected streak is a valid streak. The current algorithms on the onboard signal processor will occasionally connect a sequence of radiation events to form a streak, a false streak. A false streak will typically go through the data reduction process without being correlated and be identified as an UCT. It is necessary to separate the valid streaks from the false streaks. An algorithm has been implemented in the data reduction process to analyze streak data and identify valid streaks.

The streak detection algorithm relies on the analysis of the intensity and temporal information of the streak. Once a streak is

detected by the signal processor, a 5-pixel-wide swath encompassing the streak (Fig. 11) is sent to the ground. For each pixel in the swath, the maximum intensity value above the background average is determined, and the frame number in which it occurred is reported. Figure 12 shows a raw frameset with six valid streaks and one false streak and plots of the streak intensity along their lengths. In this case, the false streak consists of two radiation events being connected together. One discriminant is the variability of the intensity information that is quantified by dividing the standard deviation of the streak intensity by its mean. This quantity is referred to as a scintillation index. Valid streaks show less variability than false streaks. A scintillation index for the temporal information is also used, and it consists of looking at the statistics of the frame numbers occupied by the brightest pixel for each row of the streak swath. Again, valid streaks show less variability than false streaks. The intensity and frame indices are combined to form a streak quality index that is then used to separate valid and false streaks.

Once a UCT detection has been determined to be valid, further steps are taken in an effort to identify it. The first step is to determine if the streak can be correlated with something nearby. RSOs with old or poor quality element sets will typically not correlate. Figure 13 shows the case of a RSO with an old element set. It shows the detected and predicted locations of three RSOs that were in the field of view. The two objects near the center readily correlated to objects in the RSO catalog, but object 23118 did not initially correlate due to the age of the element set. It was eventually correlated by fitting the SBV observations with ground-based observations on 23118. Table 3 tabulates the data of Fig. 13.

The final example describes the first confirmed discovery of a lost object by SBV. On day 295 (1997), while observing the geosynchronous object 21821 (at 36°E longitude), SBV detected an UCT drifting through its field of view as shown in the two parts of Fig. 14 taken 23 h apart. No apparent catalog objects were candidates for its identity. Further observations indicated the object had stopped drifting, and an element set was created using initial orbit determination techniques. This element set was then refined with additional observations.

The photometric data for this object was analyzed for clues to its identity. Figure 15 shows a plot of the normalized SBV magnitude as a function of the phase angle. All observed magnitudes are normalized to a constant range of 36,000 km to remove the effect of range from the data. The curve that describes the shape of the photometric data is referred to as a phase function. The data on the UCT describes a linear phase function that is consistent with that of a large three-axis stabilized satellite whose solar panels are tracking the sun. Shown in Fig. 15, for comparison, is the suspected identity of the UCT. This UCT was suspected of being object 20705,

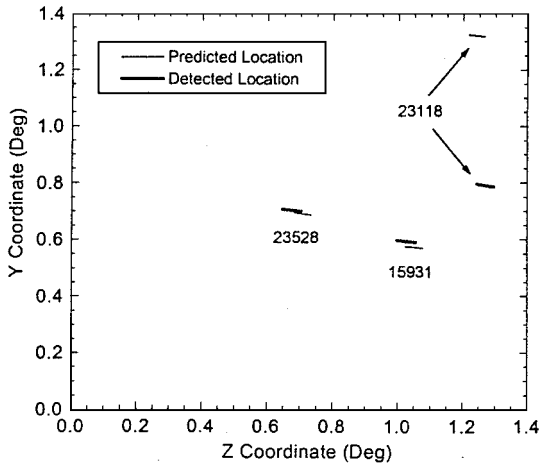

Fig. 13 Correlation of lost objects.

Table 3 Correlation of lost objects

RSO	Description	Observed SBV magnitude	Age of element set, day
23118	METEOSAT rocket body	14.5	38
15391	NATO IIID	13.3	7
23528	INTELSAT VII	11.7	<1

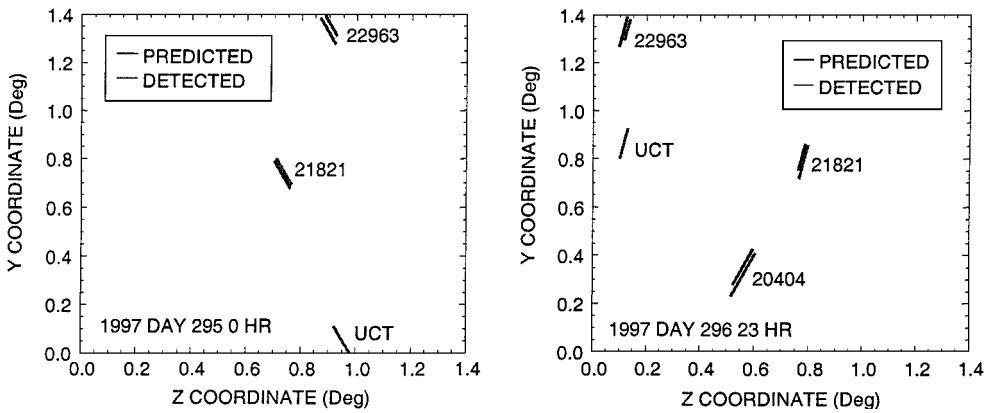

Fig. 14 SBV UCT observations.

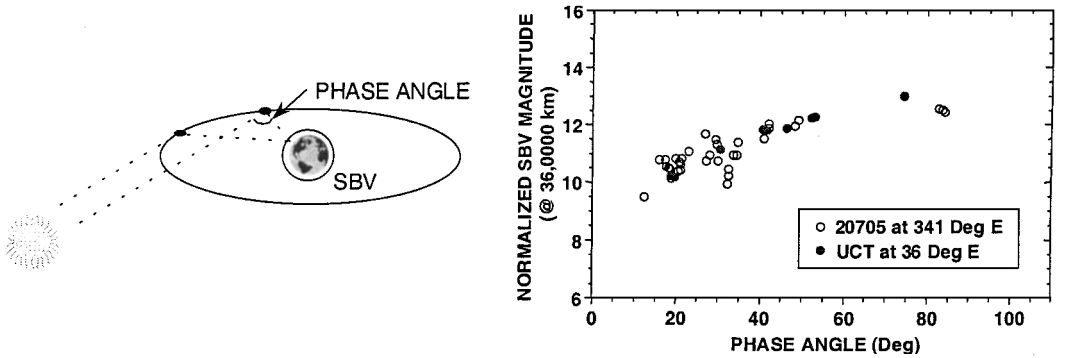

Fig. 15 UCT photometric data.

the French TDF 2 satellite (three-axis stabilized) that was being relocated from 341°E longitude. The First Command and Control Squadron was notified of the UCT, with its element set and possible identity. The object was subsequently observed by ground based sensors, and its identity was confirmed as object 20705.

Conclusion

Signal processed surveillance data collected over the first 500 days of SBV operations have been used to demonstrate the sensitivity and metric accuracy of the SBV sensor to 15th magnitude and 4 arc-s, respectively. The capability of the SBV to perform space surveillance of the entire geosynchronous belt has also been shown. The wide field of view of the SBV sensor permits simultaneous observation of geosynchronous satellite clusters and also aids in the detection of UCTs. The photometric data have proven useful in the identification of UCTs.

References

[1] Sharma, J., von Braun, C., and Gaposchkin, E. M., "Space-Based Visible Data Reduction," *Journal of Guidance, Control, and Dynamics*, Vol. 23, No. 1, 2000, pp. 171–175.

[2] Abbot, R. I., von Braun, C., and Gaposchkin, E. M., "Midcourse Space Experiment Precision Ephemeris," *Journal of Guidance, Control, and Dynamics*, Vol. 23, No. 1, 2000, pp. 187–191.

[3] von Braun, C., Sharma, J., and Gaposchkin, E. M., "Space-Based Visible Metric Accuracy," *Journal of Guidance, Control, and Dynamics*, Vol. 23, No. 1, 2000, pp. 176–182.